Inorganica Chimica Acta 399 (2013) 185–192

Contents lists available at SciVerse ScienceDirect

Inorganica Chimica Acta

journal homepage: www.elsevier.com/locate/ica

Syntheses, three types of hydrogen-bonded assembly structures, and magnetic properties of $[Fe^{III}(Him)_2(hapen)]Y\cdot solvent$ (Him = imidazole, hapen = *N,N′*-bis(2-hydroxyacetophenylidene)ethylenediamine, Y = BPh_4^-, $CF_3SO_3^-$, PF_6^-, ClO_4^-, and BF_4^-)

Masataka Koike [a], Keishiro Murakami [a], Takeshi Fujinami [a], Koshiro Nishi [a], Naohide Matsumoto [a,*], Yukinari Sunatsuki [b]

[a] Department of Chemistry, Faculty of Science, Kumamoto University, Kurokami 2-39-1, Kumamoto 860-8555, Japan
[b] Department of Chemistry, Faculty of Science, Okayama University, Tsushima-naka 1-1, Okayama 700-8530, Japan

ARTICLE INFO

Article history:
Received 28 August 2012
Received in revised form 15 November 2012
Accepted 16 January 2013
Available online 5 February 2013

Keywords:
Iron(III)
Spin equilibrium
Imidazole
N_2O_2 Schiff-base ligand
Hydrogen bonds
Assembly structures

ABSTRACT

Five iron(III) complexes of $[Fe^{III}(Him)_2(hapen)]Y\cdot solvent$ with five different counter anions were synthesized, where Him = imidazole, H_2hapen = *N,N′*-bis(2-hydroxyacetophenylidene)ethylenediamine, Y = BPh_4^- (**1**), $CF_3SO_3^-$ (**2**), PF_6^- (**3**), ClO_4^- (**4**), and BF_4^- (**5**), and solvent = methanol or H_2O. Each Fe^{III} ion has octahedral coordination geometry with N_2O_2 donor atoms of the equatorial tetradentate ligand (hapen) and two nitrogen atoms of two imidazoles at the axial positions. The imidazole group is hydrogen-bonded to the phenoxo oxygen atom of hapen of the adjacent unit and/or to the counter anion or solvent molecule, to give three types of assembly structures involving linear dimer, cyclic dimer, and one-dimensional zigzag chain. Compound **1**, with a cyclic dimer, and **2** and **3**, with a one-dimensional chain, showed spin-equilibrium behavior between high-spin ($S = 5/2$) and low-spin ($S = 1/2$) states, whereas **4** and **5**, with linear dimers, are high-spin complexes. Compound **3** shows abrupt spin transition with small thermal hysteresis.

1. Introduction

According to Tanabe–Sugano diagrams, which are based on the strong crystal-field theory of octahedral $3d^n$ metal complexes [1], the electronic ground-state changes between low-spin (LS) and high-spin (HS) states at spin crossover (SCO) points in $3d^n$ ($4 \leqslant n \leqslant 7$) metal complexes. It is known experimentally that the SCO phenomenon, interconversion between HS and LS states, is induced by external perturbations, such as temperature, pressure, pH, and light irradiation [2]. Among the SCO complexes reported so far, Fe^{II} and Fe^{III} complexes have been the most intensively studied [2,3]. It has also been recognized for a long time that the Fe sites in some heme proteins exhibit SCO behavior [4], which plays a key role in their biological functions. From the viewpoint of developing model compound of heme proteins, a number of iron porphyrins have been synthesized and studied [5]. In 1975, in order to obtain a simple SCO model compound, Nishida synthesized a family of Fe^{III} complexes with N_2O_2 Schiff-base ligands and two axial monodentate ligands, and showed that the spin states can be tuned primarily by the total ligand field strength provided by the equatorial and axial ligands [6]. For example (see Scheme 1), $[Fe^{III}(Him)_2(salen)]BPh_4$ and $[Fe^{III}(Him)_2(acacen)]BPh_4$ are HS and LS complexes, respectively, where the axial ligand was fixed as imidazole (Him), and H_2salen, H_2acacen, and BPh_4^- denote *N,N′*-bis(salicylidene)ethylenediamine, *N,N′*-bis(acetylacetonylidene) ethylenediamine, and tetraphenylborate, respectively [6]. Within the $[Fe^{III}(Him)_2L]BPh_4$ (L = N_2O_2 Schiff-base ligand) framework, salen provides a weak enough ligand field to give HS states and acacen provides a strong enough ligand field to give LS states. Later, Murray in 1987 and Real in 1998 synthesized SCO iron(III) complexes with analogous symmetrical Schiff-base ligands [7]. Matsumoto in 1984 synthesized $[Fe(Him)_2(salacen)]BPh_4$ using the unsymmetrical ligand salacen (H_2salacen = *N*-salicylidene-*N′*-acetylacetonylidene)ethylenediamine) in order to provide an intermediate ligand field strength between those provided by salen and acacen, and confirmed the spin-equilibrium properties of the complex [8]. Nishida and Matsumoto also pointed out that suitable ligand field strength of the equatorial ligand H_2L can be supplied by symmetrical Schiff-base ligands such as *N,N′*-bis(benzoylacetonylidene)ethylenediamine (H_2bzacen) and *N,N′*-bis(2-hydroxyacetophenylidene)ethylenediamine (H_2hapen), respectively [6b,8b].

In this study, using a symmetrical ligand, i.e., H_2hapen, five iron(III) complexes $[Fe^{III}(Him)_2(hapen)]Y\cdot solvent$ with five different

* Corresponding author. Tel./fax: +81 96 342 3390.
E-mail address: naohide@aster.sci.kumamoto-u.ac.jp (N. Matsumoto).

0020-1693/$ - see front matter © 2013 Elsevier B.V. All rights reserved.
http://dx.doi.org/10.1016/j.ica.2013.01.021

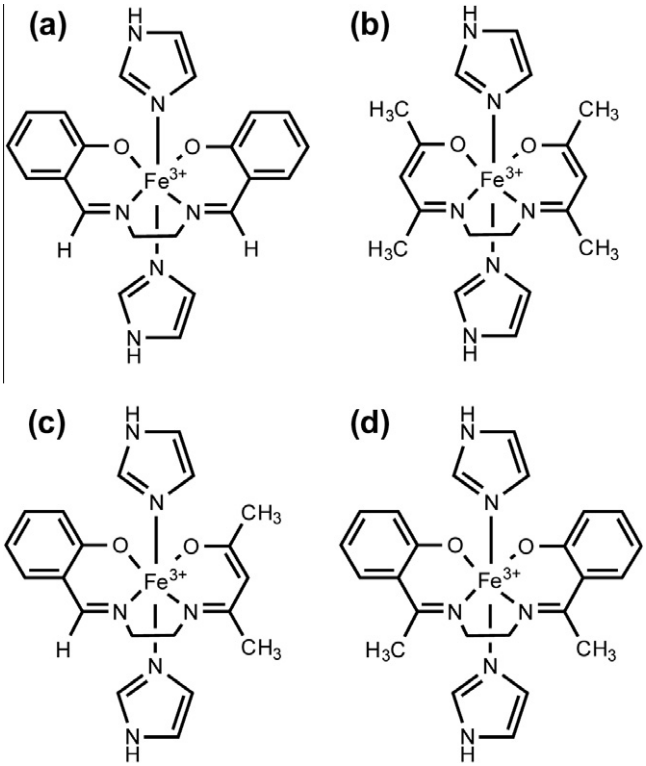

Scheme 1. Structures of $[Fe^{III}(Him)_2(salen)]^+$ (**a**), $[Fe^{III}(Him)_2(acacen)]^+$ (**b**), $[Fe^{III}(Him)_2(salacen)]^+$ (**c**), and $[Fe^{III}(Him)_2(hapen)]^+$ (**d**).

counter anions were synthesized, where Y = BPh_4^-, $CF_3SO_3^-$, PF_6^-, ClO_4^-, and BF_4^-, and solvent = crystal solvent (see Scheme 1). As the equatorial ligand H_2hapen and the axial ligand imidazole are fixed for the five complexes, and provide a ligand field strength around the SCO point, the complex-cation of $[Fe^{III}(Him)_2(hapen)]^+$ with various anions may give SCO complexes. Hence, these complexes are suitable for investigating the details of the effects of the counter anion and crystal solvent on the SCO properties. These complexes gave a variety of assembly structures, constructed by hydrogen-bonding, depending on the counter anion, and some complexes showed SCO and others did not; we report their syntheses, structures, and magnetic properties.

2. Experimental

Caution! Perchlorate salts of metal complexes are potentially explosive. Only small quantities of material should be prepared and the samples should be handled with care.

2.1. General

All reagents and solvents used in this study are commercially available from Tokyo Kasei Co., Ltd., Tokyo, Japan and Wako Pure Chemical Industries, Ltd., Osaka, Japan, and were used without further purification. All of the synthetic procedures were performed in air.

2.2. Preparation of materials

2.2.1. Preparations of tetradentate ligand H_2hapen and precursor iron(III) complex $[Fe^{III}Cl(hapen)]\cdot 0.5CH_3OH$

The tetradentate ligand, *N,N′*-bis(2-hydroxyacetophenylidene)ethylenediamine, was prepared according to the literature [9]. To a solution of 2-hydroxyacetophenone (0.1 mol, 13.63 g) in 50 mL of methanol was added a solution of ethylenediamine (0.05 mol, 3.01 g) in 50 mL of methanol, and the mixture was stirred for 1 h on a hot-plate. The resulting yellow crystalline material was collected by suction filtration, washed with a small amount of methanol, and dried in vacuo. Yield: 14.78 g (99%). Calc. for H_2hapen ($C_{18}H_{20}N_2O_2$): C, 72.95; H, 6.80; N, 9.45. Found: C, 72.93; H, 6.82; N, 9.32%. Mp = 193–196 °C. The precursor iron(III) complex $[Fe^{III}Cl(hapen)]\cdot 0.5CH_3OH$ was prepared according to the literature method [8b].

2.2.2. Preparation of iron(III) complex $[Fe^{III}(Him)_2(hapen)]Y\cdot$solvent (Y = BPh_4^- (**1**), $CF_3SO_3^-$ (**2**), PF_6^- (**3**), ClO_4^- (**4**), and BF_4^- (**5**), and solvent = methanol or H_2O)

*2.2.2.1. $[Fe^{III}(Him)_2(hapen)]BPh_4\cdot 2CH_3OH\cdot H_2O$ (**1**).* To a suspension of $[Fe^{III}Cl(hapen)]\cdot 0.5CH_3OH$ (1 mmol, 0.40 g) in 30 mL of methanol was added an excess of imidazole (10 mmol, 0.68 g), and the mixture was stirred for 10 min on a hot-plate and then filtered. To the filtrate was added a solution of $NaBPh_4$ (1 mmol, 0.34 g) in 5 mL of methanol. The resulting solution was allowed to stand for several hours, during which time dark-purple plate-like crystals precipitated, and they were collected by suction filtration and dried in air. Yield: 0.56 g (63%). Calc. for $[Fe^{III}(Him)_2(hapen)]BPh_4\cdot 2CH_3OH\cdot H_2O$ ($C_{24}H_{26}N_6O_2Fe\cdot BPh_4\cdot 2CH_3OH\cdot H_2O$): C, 67.65; H, 6.36; N, 9.47. Found: C, 67.59; H, 6.08; N, 9.90%.

*2.2.2.2. $[Fe^{III}(Him)_2(hapen)]CF_3SO_3\cdot 1.5H_2O$ (**2**).* Compound **2** was prepared using a similar method as that used to prepare **1**, using $NaCF_3SO_3$ instead of $NaBPh_4$. Yield: 0.40 g (60%). Calc. for $[Fe^{III}(Him)_2(hapen)]CF_3SO_3\cdot 1.5H_2O$ ($C_{24}H_{26}N_6O_2Fe\cdot CF_3SO_3\cdot 1.5H_2O$): C, 45.33; H, 4.41; N, 12.69. Found: C, 45.07; H, 4.39; N, 12.94%.

*2.2.2.3. $[Fe^{III}(Him)_2(hapen)]PF_6\cdot 2H_2O$ (**3**).* Compound **3** was prepared using a similar method as that used to prepare **1**, using $NaPF_6$ instead of $NaBPh_4$. Yield: 0.44 g (66%). Calc. for $[Fe^{III}(Him)_2(hapen)]PF_6\cdot 2H_2O$ ($C_{24}H_{26}N_6O_2Fe\cdot PF_6\cdot 2H_2O$): C, 43.19; H, 4.53; N, 12.59. Found: C, 43.13; H, 4.50; N, 13.05%.

*2.2.2.4. $[Fe^{III}(Him)_2(hapen)]ClO_4\cdot 0.5CH_3OH$ (**4**).* Compound **4** was prepared using a similar method as that used to prepare **1**, using $NaClO_4$ instead of $NaBPh_4$. Yield: 0.35 g (58%). Calc. for $[Fe^{III}(Him)_2(hapen)]ClO_4\cdot 0.5CH_3OH$ ($C_{24}H_{26}N_6O_2Fe\cdot ClO_4\cdot 0.5CH_3OH$): C, 48.90; H, 4.69; N, 13.96. Found: C, 48.98; H, 4.65; N, 14.32%.

*2.2.2.5. $[Fe^{III}(Him)_2(hapen)]BF_4\cdot 0.5Him\cdot H_2O$ (**5**).* Compound **5** was prepared using a similar method as that used to prepare **1**, using $NaBF_4$ instead of $NaBPh_4$. Yield: 0.38 g (60%). Calc. for $[Fe^{III}(Him)_2(hapen)]BF_4\cdot 0.5Him\cdot H_2O$ ($C_{24}H_{26}N_6O_2Fe\cdot BF_4\cdot 0.5Him\cdot H_2O$): C, 48.99; H, 4.84; N, 15.68. Found: C, 48.91; H, 4.80; N, 15.34%.

2.3. Physical measurements

Elemental analyses (C, H, and N) were carried out by Miss. Kikue Nishiyama at the Center for Instrumental Analysis of Kumamoto University. Melting points were measured by METTLE FP90 Central Processor. Magnetic susceptibilities were measured by a Quantum Design MPMS-XL5 magnetometer in the temperature range of 5–300 K at the 2 K min^{-1} under an applied magnetic field of 0.5 T. The calibration was performed with palladium metal. Corrections for diamagnetism were applied using Pascal's constants [10].

2.4. Crystallographic data collection and structure analyses

X-ray diffraction data were collected using a Rigaku RAXIS RAPID imaging plate diffractometer using graphite monochromated Mo Kα radiation (λ = 0.71073 Å). The temperature of the crystal was maintained at the selected value by means of a Rigaku cooling

device within an accuracy of ±2 K. The X-ray diffraction data for all five complexes were first collected at 296 K, and then the diffraction data at the lower temperatures for **2** and **3** were collected. The data were corrected for Lorentz, polarization and absorption effects. The structures were solved by a direct method, and expanded using the Fourier technique [11]. Some of the crystal solvents were not found on the D-Fourier. Hydrogen atoms were fixed at the calculated positions and refined using a riding model. All calculations were performed using the CrystalStructure crystallographic software package [12].

3. Results and discussion

3.1. Synthesis and characterization of iron(III) complexes [$Fe^{III}(Him)_2$(hapen)]Y·solvent [Y = BPh_4^- (**1**), $CF_3SO_3^-$ (**2**), PF_6^- (**3**), ClO_4^- (**4**), BF_4^- (**5**)]

The precursor Fe^{III} complex [Fe^{III}Cl(hapen)]·0.5CH_3OH was obtained by mixing the ligand H_2hapen, iron(III) chloride anhydrate, and triethylamine in a 1:1:2 M ratio in methanol. The Fe^{III} complexes [$Fe^{III}(Him)_2$(hapen)]Y (Y = BPh_4^- (**1**), $CF_3SO_3^-$ (**2**), PF_6^- (**3**), ClO_4^- (**4**), BF_4^- (**5**)) with two imidazoles at the axial positions and various counter anions were obtained as black plate-like crystals by mixing [Fe^{III}Cl(hapen)]·0.5CH_3OH, imidazole, and NaY (Y = BPh_4^-, $CF_3SO_3^-$, PF_6^-, ClO_4^-, BF_4^-) in a 1:10:1 M ratio in methanol. The C, H, and N elemental analyses agreed with the formula [$Fe^{III}(Him)_2$(hapen)]Y·solvent. Ground samples of complexes **1**, **2**, and **3** showed thermochromism, whereas those of **4** and **5** did not. The dark-purple color of the ground samples of **1** and **2** at room temperature changed to a greenish-black color at liquid-nitrogen temperature, and the dark-purple color of **3** at room temperature changed to black at liquid-nitrogen temperature.

3.2. Temperature-dependence of magnetic properties

The magnetic susceptibilities (χ_M) of the polycrystalline samples were measured in the temperature range 5–300 K under an applied magnetic field of 0.5 T at a sweep rate of 2 K min^{-1}. The magnetic susceptibility was measured while lowering the temperature from 300 to 5 K in the first run. Subsequently, the magnetic susceptibility was measured while raising the temperature from 5 to 300 K in the second run. The χ_MT vs. T plots for all five complexes are shown in Fig. 1. The plots for the warming and cooling modes are practically the same for all five complexes, showing no thermal hysteresis.

The experimental data were examined in terms of the spin-only values of the HS (S = 5/2) and LS (S = 1/2) states of Fe^{III} ions with the $3d^5$ electronic configuration; the theoretical spin-only χ_MT values for the HS (S = 5/2) and LS (S = 1/2) states are 4.37 and 0.375 cm^3 mol^{-1} K, respectively. The χ_MT value of **1** is 4.14 cm^3 mol^{-1} K at 300 K, which is slightly smaller than the spin-only HS value of 4.37 cm^3 mol^{-1} K. On lowering the temperature, the χ_MT value gradually decreases to 3.07 cm^3 mol^{-1} K at 5 K; this value is much larger than the spin-only LS value, showing an incomplete and very gradual spin equilibrium. The χ_MT value of **2** is 3.94 cm^3 mol^{-1} K at 300 K, which is smaller than the spin-only HS value. On lowering the temperature, the χ_MT value decreases gradually to 1.33 cm^3 mol^{-1} K at 5 K; this value is closer to the LS value than that of **1** is, but considerably larger than the LS value. Compound **2** shows a gradual spin equilibrium over a wide temperature range. Compound **3** shows a complete abrupt spin transition between the HS and LS states. The χ_MT curves in the cooling and warming modes measured at the sweeping rate of 2 K min^{-1} show a small but definite difference in the spin transition temperature region, suggesting a very small thermal hysteresis. The present abrupt spin transition with thermal hysteresis is unusual for SCO Fe^{III} complexes. The χ_MT value above 150 K of **3** has a constant value of ca. 4.4 cm^3 mol^{-1} K, which is compatible with 4.37 cm^3 mol^{-1} K of the spin-only HS value. On lowering the temperature, the χ_MT value decreases abruptly at around 75 K, and then reaches a constant value of ca. 0.7 cm^3 mol^{-1} K below 40 K; this value is comparable to the LS (S = 1/2) spin-only value and those of the reported LS Fe^{III} complexes. The spin-transition temperature is evaluated by calculating the derivative of $\delta\chi_MT$ vs δT, giving $T_{1/2}$ = 78 K.

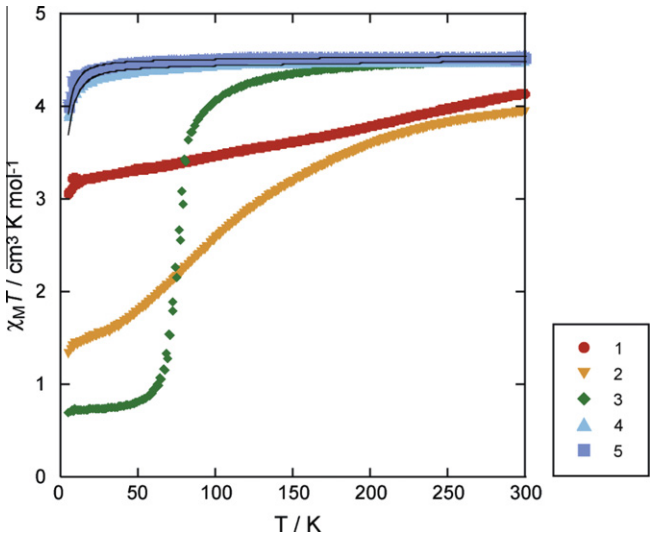

Fig. 1. χ_MT vs. T plots for complexes **1**–**5**, showing their various magnetic properties; **1** BPh_4^- (●); **2** $CF_3SO_3^-$ (▼); **3** PF_6^- (◆); **4** ClO_4^- (■); and **5** BF_4^- (▲). The solid lines for **4** and **5** represent the theoretical curves with the fitting parameters given in the text.

Compounds **4** and **5** show essentially similar magnetic behaviors to each other. In the higher temperature region above ca. 40 K, the compounds have constant χ_MT values of ca. 4.4 cm^3 mol^{-1} K, which is compatible with the expected HS value of S = 5/2. The χ_MT value decreases abruptly below 20 K. This abrupt decrease in the magnetic behavior cannot be ascribed to spin transitions from HS to LS states, but is caused by second-order Zeeman effects for $(t_{2g})^3(e_g)^2$ species in axially distorted octahedral surroundings [10,13]. These magnetic behaviors can be analyzed using Eq. (1) [10,14]. Eq. (1), for the average magnetic susceptibility, takes account of single-ion anisotropy, where g_{Fe} is the Lande g factor for the Fe ion, k_B is Boltzmann's constant, β is the Bohr magneton, $x = D/k_BT$, where the parameter D is a measure of the zero-field splitting, and $N\alpha$ is the temperature-independent paramagnetism [14].

$$<\chi> = Ng_{Fe}^2\beta^2/12k_BT(19 + 16/x + (9 - 11/x)e^{-2x} + (25 - 5/x)e^{-6x})/(1 + e^{-2x} + e^{-6x}) + N\alpha \quad (1)$$

The value of was used. The best fit was obtained when g_{Fe} = 2.01, D = 4.5 cm^{-1}, and $N\alpha = 2.5 \times 10^{-4}$ cm^3 mol^{-1} for **4**, and for corresponding values of 2.027, 3.5 cm^{-1}, and $N\alpha = 1.7 \times 10^{-4}$ cm^3 mol^{-1} for **5**. The obtained fitting values are typical of slightly distorted octahedral high-spin iron(III) environments [14].

3.3. Crystal structures

3.3.1. Crystal structures of **1**–**5** at 296 K

The crystal structures of **1**–**5** were determined using single-crystal X-ray diffraction at several temperatures. The crystallographic data are listed in Table 1. Relevant coordination bond distances and angles, and hydrogen-bond distances are given in

Table 1
Crystallographic data for BPh_4^- salt (**1**), $CF_3SO_3^-$ salt (**2**), PF_6^- salt (**3**), ClO_4^- salt (**4**), and BF_4^- salt (**5**).

	BPh_4 (**1**)	CF_3SO_3 (**2**)			PF_6 (**3**)			ClO_4 (**4**)	BF_4 (**5**)
Formula	$C_{50}H_{54}N_6O_4FeB$	$C_{25}H_{26}N_6O_5FeF_3$			$C_{24}H_{26}N_6O_2FePF_6$			$C_{24.5}H_{28}N_6O_6FeCl$	$C_{25.5}H_{30}N_7O_3FeBF_4$
Formula weight	869.67	635.42			631.32			601.83	607.20
Crystal system	triclinic	monoclinic			monoclinic			triclinic	triclinic
Space group	$P\bar{1}$ (No. 2)	$C2/c$ (No. 15)			$C2/c$ (No. 15)			$P\bar{1}$ (No. 2)	$P\bar{1}$ (No. 2)
T (K)	296	296	200	103	296	200	103	296	296
a (Å)	12.120(7)	24.668(2)	24.415(1)	24.209(1)	24.333(5)	24.250(2)	24.085(1)	9.6826(7)	9.678(2)
b (Å)	12.658(7)	9.6459(7)	9.5785(4)	9.5144(3)	9.636(2)	9.5816(5)	9.5517(4)	15.345(2)	15.557(3)
c (Å)	15.544(9)	25.208(3)	25.0179(9)	24.8577(8)	25.094(4)	24.823(2)	24.596(1)	18.770(2)	18.599(3)
α (°)	96.103(7)	90	90	90	90	90	90	77.616(3)	78.512(4)
β (°)	104.876(6)	113.893(2)	113.502(2)	113.186(2)	113.557(5)	113.054(2)	112.746(2)	84.515(2)	85.155(4)
γ (°)	97.521(6)	90	90	90	90	90	90	82.917(2)	83.697(4)
V (Å^3)	2260(3)	5484.2(8)	5365.4(4)	5263.1(4)	5394(2)	5307.2(6)	5218.3(4)	2696.3(4)	2722.3(8)
Z	2	8			8			4	4
D_{calcd} (g cm^{-3})	1.278	1.539	1.573	1.604	1.555	1.580	1.607	1.482	1.481
μ (mm^{-1})	3.848	6.938	7.091	7.229	6.941	7.054	7.174	7.108	6.189
R^a, Rw^b	0.0730, 0.1612	0.0739, 0.2129	0.0694, 0.2159	0.0702, 0.2158	0.0870, 0.2396	0.0730, 0.2197	0.0756, 0.2239	0.0908, 0.2519	0.1047, 0.2885

[a] $R = \sum||F_o| - |F_c||/\sum|F_o|$.
[b] $Rw = [\sum w(|F_o^2| - |F_c^2|)^2/\sum w|F_o^2|^2]^{1/2}$.

Table 2
Coordination bond distances (Å) and angles (°) for BPh_4^- salt (**1**), $CF_3SO_3^-$ salt (**2**), and PF_6^- salt (**3**).

	BPh_4 (**1**)	CF_3SO_3 (**2**)			PF_6 (**3**)		
	296 K	296 K	200 K	103 K	296 K	200 K	103 K
Fe–N1	1.969(6)	2.107(6)	2.080(6)	2.039(5)	2.105(7)	2.102(6)	2.092(7)
Fe–N2	1.984(7)	2.088(5)	2.070(4)	2.026(4)	2.127(5)	2.118(5)	2.101(5)
Fe–N3	2.033(8)	2.141(4)	2.118(4)	2.073(4)	2.164(5)	2.159(4)	2.130(4)
Fe–N5	2.034(8)	2.143(4)	2.129(4)	2.086(4)	2.144(5)	2.143(5)	2.129(5)
Fe–O1	1.858(6)	1.880(4)	1.881(3)	1.881(3)	1.883(4)	1.890(4)	1.879(4)
Fe–O2	1.861(5)	1.898(5)	1.900(5)	1.893(5)	1.890(6)	1.903(6)	1.907(6)
<Fe–N>	2.005	2.120	2.099	2.056	2.135	2.131	2.114
O1–Fe–O2	91.8(3)	101.50(17)	99.69(16)	95.83(15)	101.9(2)	101.66(18)	100.5(2)
O1–Fe–N1	91.3(3)	88.06(18)	88.70(17)	89.88(16)	88.5(3)	88.62(19)	89.1(2)
O1–Fe–N3	90.1(3)	92.38(15)	92.35(14)	92.04(14)	92.21(18)	92.83(16)	93.32(17)
O1–Fe–N5	87.7(3)	91.87(15)	91.99(14)	91.78(13)	93.49(19)	93.27(15)	93.20(17)
O2–Fe–N2	91.8(3)	89.1(2)	89.73(18)	90.92(17)	88.7(3)	88.8(2)	89.1(2)
O2–Fe–N3	89.4(3)	90.08(17)	89.62(17)	89.10(15)	89.9(3)	89.36(19)	89.0(2)
O2–Fe–N5	92.0(3)	91.57(19)	91.78(18)	91.39(16)	92.6(3)	92.8(2)	92.6(2)
N1–Fe–N2	85.3(3)	81.4(2)	81.94(19)	83.41(18)	80.9(3)	81.0(2)	81.4(3)
N1–Fe–N3	87.7(3)	87.76(18)	88.30(17)	89.10(16)	87.5(3)	87.89(18)	88.5(2)
N1–Fe–N5	91.1(3)	89.84(19)	89.64(18)	90.02(17)	88.8(3)	88.8(2)	88.8(2)
N2–Fe–N3	92.8(3)	89.27(16)	89.41(15)	89.52(15)	88.87(18)	88.39(2)	87.77(17)
N2–Fe–N5	89.3(3)	86.08(16)	85.95(15)	86.59(14)	84.8(2)	84.99(16)	85.33(17)

Table 3
Hydrogen bond distances (Å) for BPh_4^- salt (**1**), $CF_3SO_3^-$ salt (**2**), and PF_6^- salt (**3**) at 296 K.

BPh_4^- salt (**1**)	
N6*···O4	2.800(11)
O1···O3	2.821(11)
O3···O4	2.626(10)
$CF_3SO_3^-$ salt (**2**)	
N6*···O2	2.911(7)
N4···O8	2.887(17)
PF_6^- salt (**3**)	
N6*···O2	2.938(8)

Table 2 and 3 for **1-3** and in Table 4 for **4** and **5**. Compound **1** crystallized in a triclinic space group, $P\bar{1}$ (No. 2), and the unique crystallographic unit consists of one $[Fe^{III}(Him)_2(hapen)]^+$, two methanol molecules as the crystal solvent, and one BPh_4^- anion. Compounds **2** and **3** crystallized in an isomorphous monoclinic space group, $C2/c$, and each unique unit consists of one $[Fe^{III}(Him)_2(hapen)]^+$, two methanol molecules as the crystal solvent, and one counter anion, i.e., $CF_3SO_3^-$, for **2** and PF_6^- for **3**. Compounds **4** and **5** have isomorphous structures and crystallized in a triclinic space group, $P\bar{1}$ (No. 2), with $Z = 4$, and the unique unit consists of two $[Fe^{III}(Him)_2(hapen)]^+$ complex cations, two counter anions, and crystal solvent molecules (see Table 4).

The molecular structures of all the cationic part of compounds **1**–**5** are similar to each other. The molecular structure of the $[Fe^{III}(Him)_2(hapen)]^+$ part of **1**, and the atom numbering scheme, are shown in Fig. 2, as a representative example. The Fe^{III} ion of the complex cation has an octahedral coordination environment with the N_2O_2 donor atoms of the equatorial tetradentate ligand hapen, and N_2 donors of two imidazoles at the axial positions. The Fe–N and Fe–O coordination bond distances are indicative of the spin state. These Fe–N and Fe–O coordination bond distances in all five complexes at 296 K are consistent with the reported bond lengths for HS iron(III) complexes with similar Schiff-base ligands [6c,7,8]. The relative orientation of the imidazole rings is one of the parameters that determine the coordination core bond lengths and consequently the spin state [3]. Fig. 2(b) shows the orientations of the two imidazole rings, in which one imidazole ring bisects the angles defined by the two N–Fe–O diagonals, and the other imidazole ring is oriented nearly along the N–Fe–O diagonal.

Table 4
Coordination bond distances and hydrogen bond distances and bond angle for ClO_4^- salt (**4**) and BF^- salt (**5**) at 296 K.

	ClO_4	BF_4
Bond distance		
Fe1–N1	2.119(8)	2.113(7)
Fe1–N2	2.116(8)	2.114(7)
Fe1–N3	2.172(7)	2.174(7)
Fe1–N5	2.142(7)	2.150(6)
Fe1–O1	1.899(7)	1.871(6)
Fe1–O2	1.909(6)	1.913(6)
Fe1–N average	2.137	2.138
Fe2–N7	2.114(8)	2.122(7)
Fe2–N8	2.093(7)	2.096(7)
Fe2–N9	2.146(8)	2.137(7)
Fe2–N11	2.159(8)	2.156(7)
Fe2–O3	1.881(6)	1.858(5)
Fe2–O4	1.918(6)	1.931(5)
Fe2–N average	2.128	2.128
Hydrogen bond distance		
N6···O4	2.795(10)	2.787(9)
N4···O18 or F10	2.60(2)	2.676(18)
N12···O6 or F2	2.776(12)	2.681(16)
N10···N13 or O19	2.96(3)	2.772(13)
Bond angle		
O1–Fe1–O2	104.5(3)	104.2(3)
O1–Fe1–N1	88.1(3)	87.7(3)
O1–Fe1–N3	93.4(3)	94.3(3)
O1–Fe1–N5	89.7(3)	90.3(3)
O2–Fe1–N2	87.1(3)	87.4(3)
O2–Fe1–N3	91.8(3)	91.9(3)
O2–Fe1–N5	94.0(3)	94.6(3)
N1–Fe1–N2	80.2(3)	80.6(3)
N1–Fe1–N3	88.6(3)	87.5(3)
N1–Fe1–N5	84.8(3)	84.8(3)
N2–Fe1–N3	87.1(3)	86.1(3)
N2–Fe1–N5	88.4(3)	87.8(3)
O3–Fe2–O4	103.8(3)	103.5(2)
O3–Fe2–N7	88.4(3)	88.2(3)
O3–Fe2–N9	94.2(3)	95.4(3)
O3–Fe2–N11	91.0(3)	91.0(3)
O4–Fe2–N8	87.2(3)	87.7(3)
O4–Fe2–N9	88.3(3)	88.7(3)
O4–Fe2–N11	94.6(3)	95.0(3)
N7–Fe2–N8	80.6(3)	80.7(3)
N7–Fe2–N9	88.2(3)	87.4(3)
N7–Fe2–N11	87.7(3)	87.6(3)
N8–Fe2–N9	87.1(3)	86.3(3)
N8–Fe2–N11	87.0(3)	86.4(3)

Similar relative orientations of the two imidazole rings are found for the other complexes.

The spin sate of $[Fe^{III}(salX)(L)^2]^+$ systems (salX = N_2O_2 Schiff-base ligand; L = pyridine or imidazole) has been explained by the structural parameters. For example, the O–Fe–O bond angles of the equatorial coordination plane at 296 K are indicative of the spin state; high-spin compounds **4** and **5** have the large angle around 103.5°, while SCO compounds **1**, **2** and **3** have smaller angles of 91.8°, 101.5° and 101.9°, respectively. Murray et al. demonstrated that the five-membered chelate ring involving ethylenediamine moiety is closely related to the spin state, (1) the envelope conformation accepts the spin transition; (2) the gaushe or planar conformation locks in high spin state [15]. Compounds **4** and **5** of high-spin complexes have a gaushe conformation, while the other compounds of SCO complexes **1**–**3** are closer to an envelope conformation, giving a distortion of two benzene moieties. This result is accord with that of Murray [15].

3.3.2. Three types of hydrogen-bonded assembly structures

As shown in Table 1, compounds **1**–**5** crystallized in three types of crystal structures: **1** crystallized in a triclinic space group, $P\bar{1}$ (No. 2); **2** and **3** crystallized in an isomorphous monoclinic space group, $C2/c$; and **4** and **5** crystallized in an isomorphous triclinic space group, $P\bar{1}$ (No. 2), with $Z = 4$. As described below, three types of hydrogen-bonded assembly structures are generated.

Fig. 3 shows the cyclic dimer structure, $\{\cdots[Fe^{III}(Him)_2(hapen)]\cdots(MeOH)\cdots(MeOH)\cdots\}_2$, of **1**. The cyclic dimer structure has an inversion center consisting of two Fe^{III} complex molecules, i.e., $[Fe^{III}(Him)_2(hapen)]^+$, and four methanol molecules. One of the two phenoxo oxygen atoms of hapen in the complex cation, O(1), is hydrogen-bonded to the oxygen atom O(3) of the methanol molecule, with a distance of O(1)···O(3) = 2.821(11) Å. The oxygen atom O(3) of methanol is further hydrogen-bonded to another methanol, with a distance of O(3)···O(4) = 2.626(10) Å. The oxygen atom O(4) is further hydrogen-bonded to a nitrogen atom N(6)* of the coordinated imidazole of the adjacent complex unit, with a distance of O(4)···N(6)* = 2.800(11) Å. As a result, a cyclic dimeric structure, $\{\cdots[Fe^{III}(Him)_2(hapen)]\cdots(MeOH)\cdots(MeOH)\cdots\}_2$, is constructed by hydrogen-bonds. The BPh_4^- ion is not involved in the cyclic dimer structure, and is present as the counter anion. The same cyclic structure was found in $[Fe^{III}((Him)_2(hapacen)]BPh_4{\cdot}2MeOH$ [16], which showed spin equilibrium, where hapacen = *N*-(2-hydroxyacetophenylidene)-*N*′-(acetylacetonylidene)ethylenediamine.

As the crystal structures of **2** and **3** are isomorphous, these two complexes have essentially the same crystal structures. Fig. 4(a) and (b) show parts of one-dimensional (1D) zigzag-chain structures of **2** and **3**, respectively. The 1D structure is constructed by intermolecular hydrogen-bonding between a phenoxo oxygen, O(2), of the complex cation and an imidazole nitrogen, N(6)*, of the adjacent complex cation, with a distance of O(2)···N(6)* = 2.911(7) Å for **2** and O(2)···N(6)* = 2.938(8) Å for **3**. The adjacent complex cations are related by a two-fold screw axis along the *b*-axis and the O(2)···N(6)* hydrogen-bond is repeated to form a 1D structure running along the *b*-axis. The remaining imidazole of the two imida-

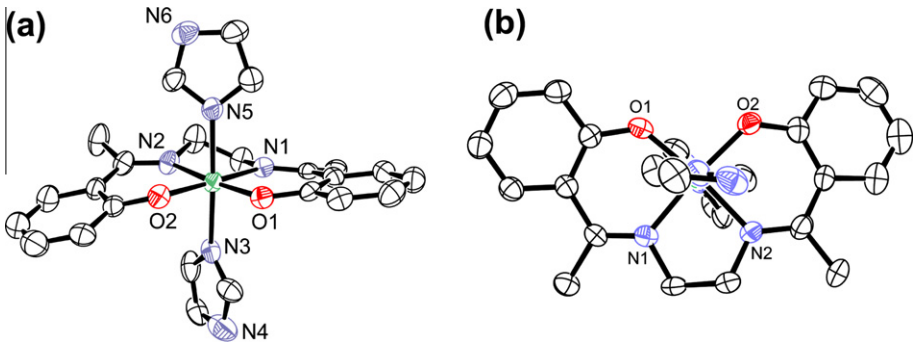

Fig. 2. (a) ORTEP drawing of $[Fe^{III}(Him)_2(hapen)]^+$ part of **1**, with the atom numbering scheme, at 200 K; the same atom numbering is used for **1**–**3**. The thermal ellipsoids were drawn at the 50% probability level. (b) View of the complex cation **1** projected on the planar tetradentate Schiff-base ligand at 296 K, showing the orientations of two imidazole rings.

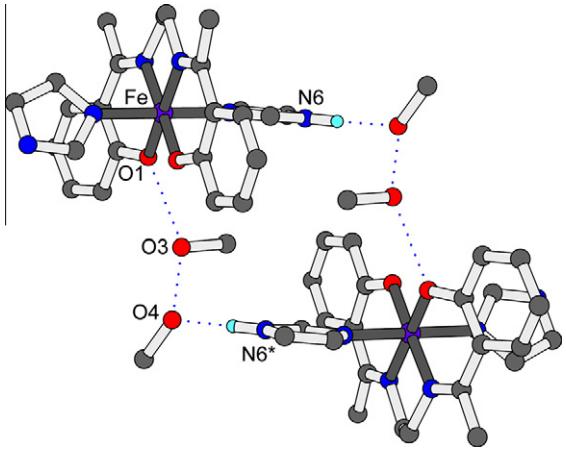

Fig. 3. Cyclic dimer structure, $\{\cdots[Fe(Him)_2(hapen)]\cdots(MeOH)\cdots(MeOH)\cdots\}_2$, of BPh_4^- salt (**1**). The structure has an inversion center and is constructed from three kinds of hydrogen-bond: O(1)···O(3) (phenoxo···methanol), O(3)···O(4) (methanol···methanol), and O(4)···N(6) (methanol···imidazole).

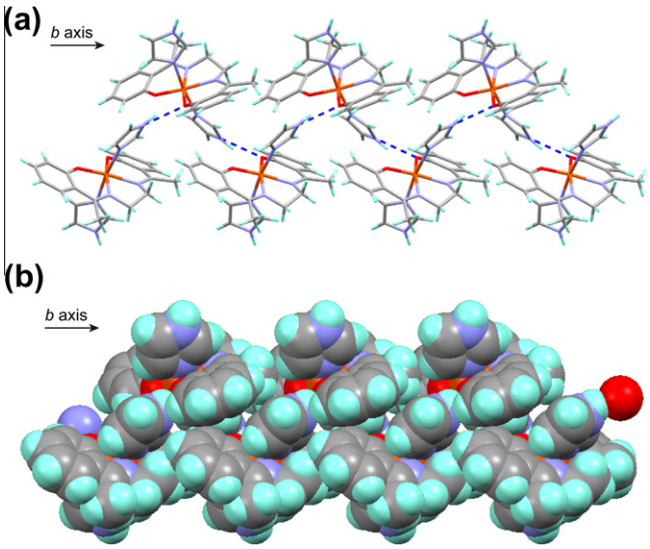

Fig. 5. (a) 1D zigzag-chain structure running along the *b*-axis of PF_6^- salt (**3**). (b) Space filling representation of the rod-like chain.

zoles per complex cation is hydrogen-bonded to the counter anion $CF_3SO_3^-$ in **2**, but is not hydrogen-bonded to PF_6^- in **3**.

The two adjacent complex-cations are related by a 2_1 screw axis along the *b*-axis and the resulting infinite 1D chain runs along the *b*-axis. Each equatorial coordination plane and axially coordinated imidazole group are tilted from the *b*-axis. Fig. 5 shows the 1D structure and its space filling representation, showing a rod-like structure. In the crystal lattice, rods are stacked along the *b*-axis, and the anions occupy the space among the rods. A similar 1D structure was found in $[Fe^{III}(4\text{-}NH_2Py)(L)]BPh_4$; 4-$NH_2$Py = 4-aminopyridine, L = bis(3-methoxysalicylideneaminopropyl)amine)] [17], in which a 1D chain was formed by intermolecular amine···phenoxo hydrogen-bonds, and the compound showed an abrupt spin transition.

As **4** and **5** are isomorphous, these two complexes have essentially the same crystal structure. Fig. 6(a) and (b) show the linear dimer structures of **4** and **5**, respectively. The linear dimer structure is constructed by hydrogen-bonds between an imidazole nitrogen, N(6), of the Fe1 site and a phenoxo oxygen, O(4), of the adjacent complex cation Fe2 site, with a distance of O(4)···N(6) = 2.794(10) Å. As a result of the O(4)···N(6) hydrogen-bond, the coordination bond distance of Fe1–O(2) is longer than that of Fe1–O(1). As shown in Fig. 6(a) and (b), the Fe1 and Fe2 sites have different hydrogen-bonding environments. One imidazole of the Fe2 site is hydrogen-bonded to the counter anion, and the other imidazole of the Fe2 site is hydrogen-bonded to, or in weak contact with, the methanol crystal solvent for **4**, and an imidazole incorporated in the crystallization for **5**. In contrast, one imidazole of the Fe1 site is hydrogen-bonded to the phenoxo oxygen of the Fe2 site to form a linear dimer structure, and the other imidazole of the Fe1 site is hydrogen-bonded to the counter anion.

3.3.3. Structural deformation during spin transition

Compounds **2** and **3** showed spin equilibrium, and their crystal structures at several temperatures were determined. The relevant coordination bond distances are summarized in Table 2. The Fe–N coordination bond distances of **2** at 296 K are is in the range 2.088(5)–2.143(4) Å; these values are in the expected range for HS Fe^{III} complexes with a Schiff-base N_4O_2 environment [3]. The corresponding distances at 103 K are in the range 2.026(4)–2.086(4); these values are shorter than those at 296 K, but are longer than those expected for the LS Fe^{III} complexes [3]. As a result of the incomplete spin transitions for **2**, the differences between the average Fe–N bond distances at 296 and 103 K are less than 0.1 Å.

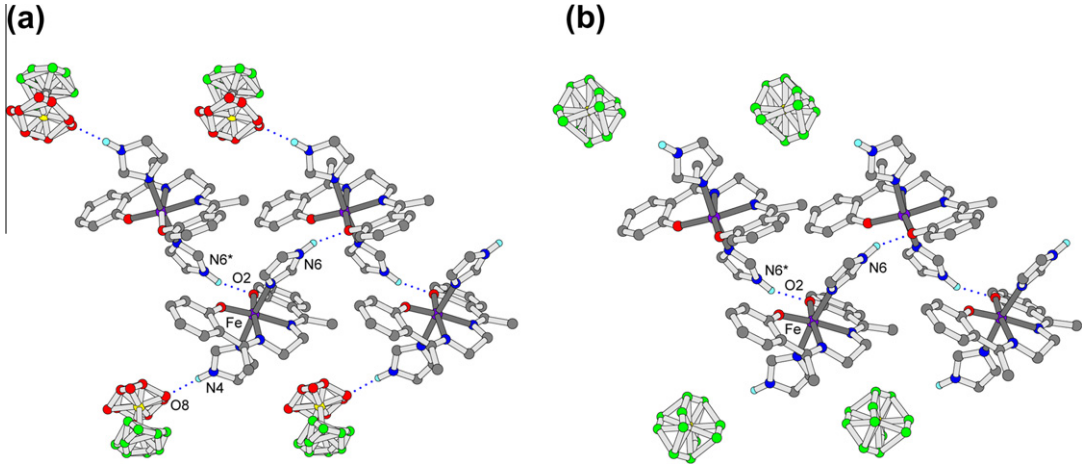

Fig. 4. (a) 1D zigzag-chain structure running along the *b*-axis of $CF_3SO_3^-$ salt (**2**). (b) 1D zigzag-chain structure running along the *b*-axis of PF_6^- salt (**3**). Anions $CF_3SO_3^-$ and PF_6^- of **1** and **2** are disordered.

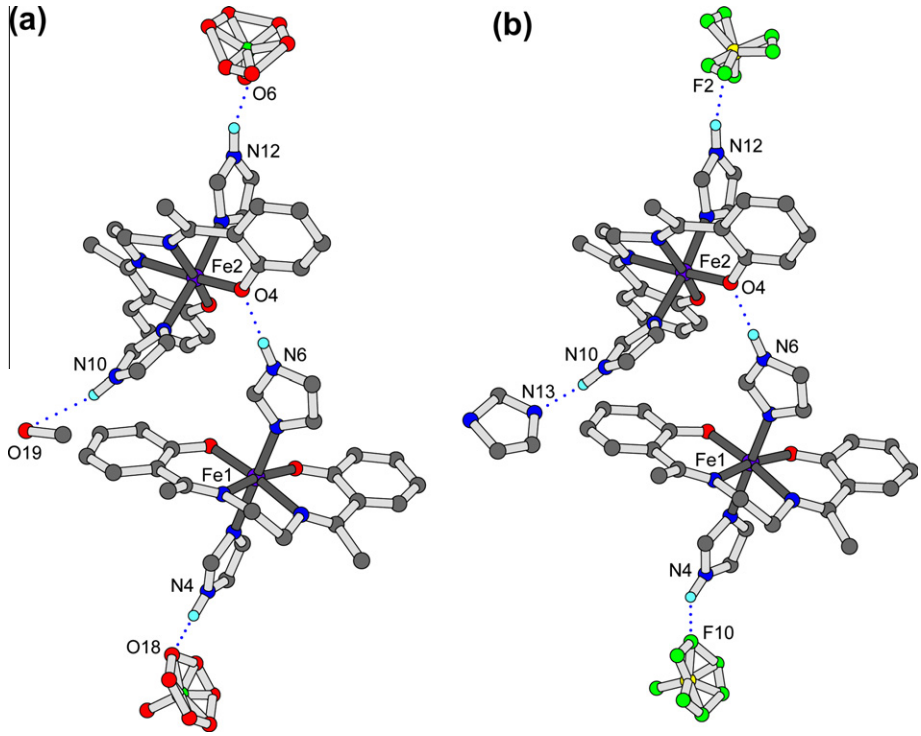

Fig. 6. (a) Linear dimer structure of ClO_4^- salt (**4**). (b) Linear dimer structure of BF_4^- salt (**5**). The structure consists of two Fe sites, Fe1 and Fe2, with different hydrogen-bonding environments. Anions ClO_4^- and BF_4^- of **4** and **5** are disordered.

The Fe–N(axial imidazole) distances change more significantly than those of Fe–N(equatorial). The spin-transition temperature of **3** (ca. 78 K) is lower than 103 K, the lowest temperature of our X-ray apparatus, and the Fe–N coordination bond distances at 296, 200, and 103 K are in the expected range for HS Fe^{III} complexes.

4. Concluding remarks

Firstly the present study is carried out from these general viewpoints on SCO complexes.

A series of complexes with the formula $[Fe^{III}(Him)_2(hapen)]Y$ were synthesized, where the metal-complex cation of $[Fe^{III}(Him)_2(hapen)]^+$ was fixed, and the molecular size and/or molecular shape of the counter anion Y varied, i.e., 86.9 $Å^3$ ($CF_3SO_3^-$), 73.0 $Å^3$ (PF_6^-), 54.4 $Å^3$ (ClO_4^-), and 53.4 $Å^3$ (BF_4^-) [18a]. The crystal packing of an SCO molecule in a crystal lattice significantly affects the SCO properties [3a]. The counter anion [18] and the solvent molecule [19] in the crystal lattice influence SCO properties caused by the molecular expansion and shrinkage indirectly but significantly. The cation and anion packing in the crystal lattice depend on the anion size and, as a result, three types of hydrogen-bonded assembly structures are generated: a SCO cyclic dimer in **1**, SCO 1D chains in **2** and **3**, and high-spin linear dimers in **4** and **5**. Compound **3**, in particular, shows a complete and abrupt spin transition with small thermal hysteresis. As five complexes contain the same complex-cation of $[Fe^{III}(Him)_2(hapen)]^+$, whose Fe^{III} ion is coordinated by N_4O_2 donor atoms of equatorial hapen and two axial Him, the variety of their magnetic properties should be preliminary related to three types of hydrogen-bonded assembly structures. It has been recognized that weak intermolecular interactions such as hydrogen-bonding play important roles in SCO properties [20]. This work provides another example of intermolecular hydrogen-bonding significantly influencing the SCO properties. It should be especially emphasized that compound **3** with 1D chain shows abrupt spin transition with thermal hysteresis, which are unusual for Fe^{III} complexes. Within a 1D chain constructed by intermolecular imidazole···phenoxo hydrogen bond, each equatorial coordination plane and imidazole group concerning with the hydrogen bond of the SCO site are tilted from the 1D axis (*b*-axis). Since the molecular volume resulting from elongation of the metal–ligand distances and the coordination geometry of individual SCO molecules changes substantially during the spin transition, such structural features can absorb the structural change raised from spin transition. By adapting this molecular design, SCO Fe(III) complex with larger thermal hysteresis can be realized.

Acknowledgments

T. Fujinami and K. Nishi were supported by the Research Fellowship for Young Scientists of the Japan Society for the Promotion of Science, KAKENHI 00248556 and 00248498.

Appendix A. Supplementary data

CCDC 897460–897468 contain the supplementary crystallographic data for $[Fe^{III}(Him)_2(hapen)]Y{\cdot}$solvent (Y = BPh_4^- (**1**), $CF_3SO_3^-$ (**2**), PF_6^- (**3**), ClO_4^- (**4**), and BF_4^- (**5**)). These data can be obtained free of charge from The Cambridge Crystallographic Data Centre via www.ccdc.cam.ac.uk/data_request/cif. Supplementary data associated with this article can be found, in the online version, at http://dx.doi.org/10.1016/j.ica.2013.01.021.

References

[1] (a) Y. Tanabe, S. Sugano, J. Phys. Soc. Jpn. 9 (1954) 766;
(b) Y. Tanabe, S. Sugano, J. Phys. Soc. Jpn. 11 (1956) 864.
[2] (a) H.A. Goodwin, Coord. Chem. Rev. 18 (1976) 293;
(b) E. König, Prog. Inorg. Chem. 35 (1987) 527;
(c) P. Gütlich, Y. Garcia, T. Woike, Coord. Chem. Rev. 219–221 (2001) 839;
(d) P. Gütlich, A. Hauser, H. Spiering, Angew. Chem., Int. Ed. 33 (1994) 2024;
(e) P. Gütlich, Y. Garcia, H.A. Goodwin, Chem. Soc. Rev. 29 (2000) 419.
[3] (a) P. Gütlich, H.A. Goodwin, Spin Crossover in Transition Metal Compounds I–III, Topics in Current Chemistry, 233–235, Springer, New York, 2004;

(b) J.A. Real, A.B. Gaspar, V. Niel, M.C. Muñoz, Dalton Trans. (2005) 2062;
(c) M.A. Halcrow, Chem. Soc. Rev. 37 (2008) 278.
[4] (a) A.H. Ewald, R.L. Martin, I.G. Ross, A.H. White, Proc. Roy. Soc. A 280 (1984) 235;
(b) G. Harris, Theor. Chim. Acta 5 (1966) 379;
(c) M. Zerner, M. Gouterman, H. Kobayashi, Theor. Chim. Acta 6 (1966) 363.
[5] (a) J.P. Collman, T.N. Sorrell, K.O. Hodgson, A.K. Kulshrestha, C.E. Strouse, J. Am. Chem. Soc. 99 (1977) 5180;
(b) J.P. Collman, X. Zhang, K. Wong, J.I. Brauman, J. Am. Chem. Soc. 116 (1994) 6245;
(c) D.H. Busch, N.W. Alcock, Chem. Rev. 94 (1994) 585;
(d) W.R. Scheidt, D.K. Geiger, R.G. Hayes, G. Lang, J. Am. Chem. Soc. 105 (1983) 2625;
(e) D.K. Geiger, Y.J. Lee, W.R. Scheidt, J. Am. Chem. Soc. 106 (1984) 6339.
[6] (a) Y. Nishida, S. Oshio, S. Kida, Chem. Lett. (1975) 79;
(b) Y. Nishida, S. Oshio, S. Kida, Bull. Chem. Soc. Jpn. 50 (1977) 119;
(c) Y. Nishida, K. Kino, S. Kida, J. Chem. Soc., Dalton Trans. (1987) 1157.
[7] (a) B.J. Kennedy, A.C. McGrath, K.S. Murray, B.W. Skelton, A.H. White, Inorg. Chem. 26 (1987) 483;
(b) R. Hernandenz-Molina, A. Mederos, S. Dominguez, P. Gili, C. Ruiz-Perez, A. Castineiras, X. Solans, F. Lloret, J.A. Real, Inorg. Chem. 37 (1998) 5102.
[8] (a) N. Matsumoto, K. Kimoto, A. Ohyoshi, Y. Maeda, Chem. Lett. (1984) 79;
(b) N. Matsumoto, K. Kimoto, A. Ohyoshi, Y. Maeda, Bull. Chem. Soc. Jpn. 57 (1984) 3307;
(c) Y. Maeda, Y. Takashima, N. Matsumoto, A. Ohyoshi, J. Chem. Soc., Dalton Trans. (1986) 1115.
[9] Y. Nakao, N. Nonagase, A. Nakahara, Bull. Chem. Soc. Jpn. 42 (1969) 452.
[10] O. Kahn, Molecular Magnetism, VCH, Weinheim, Germany, 1993.
[11] SIR92, (a) A. Altomare, G. Cascarano, C. Giacovazzo, A. Guagliardi, M. Burla, G. Polidori, M. Camalli, J. Appl. Crystallogr. 27 (1994) 435;
. DIRDIF-99,(b) P.T. Beurskens, G. Admiraal, G. Beurskens, W.P. Bosman, R. de Gelder, R. Israel, J.M.M. Smits, The DIRDIF-99 Program System, Technical Report of the Crystallography Laboratory, University of Nijmegen, The Netherlands, 1999.
[12] CrystalStructure 4.0: Crystal Structure Analysis Package, Rigaku Corporation (2000–2010), Tokyo, Japan.
[13] F.E. Mabbs, D.J. Machin, Magnetism and Transition Metal Complexes, Chapman and Hall, London, 1973.
[14] M. Gomez-Gallego, I. Fernandez, D. Pellico, A. Gutierrez, M.A. Sierra, J.J. Lucena, Inorg. Chem. 45 (2006) 5321.
[15] T.M. Ross, S.M. Neville, D.S. Innes, D.R. Turner, B. Moubaraki, K.S. Murray, J. Chem. Soc., Dalton Trans. 39 (2010) 149.
[16] T. Fukukai, K. Yabe, Y. Ogawa, N. Matsumoto, J. Mrozinski, Bull. Chem. Soc. Jpn. 78 (2005) 1484.
[17] K. Tanimura, R. Kitashima, N. Brefuel, M. Nakamura, N. Matsumoto, S. Shova, J.P. Tuchagues, Bull. Chem. Soc. Jpn. 78 (2005) 1279.
[18] (a) M. Yamada, H. Hagiwara, H. Torigoe, N. Matsumoto, M. Kojima, F. Dahan, J.P. Tuchagues, N. Re, S. Iijima, Chem. Eur. J. 12 (2006) 4536;
(b) Y. Ikuta, M. Ooidemizu, Y. Yamahata, M. Yamada, S. Osa, N. Matsumoto, S. Iijima, Y. Sunatsuki, M. Kojima, F. Dahan, J.P. Tuchagues, Inorg. Chem. 42 (2003) 7001.
[19] (a) T. Sato, K. Nishi, S. Iijima, M. Kojima, N. Matsumoto, Inorg. Chem. 48 (2009) 7211;
(b) T. Sato, S. Iijima, M. Kojima, N. Matsumoto, Chem. Lett. (2009) 178.
[20] (a) B. Weber, Coord. Chem. Rev. 253 (2009) 2432;
(b) B. Weber, W. Bauer, T. Pfaffeneder, M.M. Dirtu, A.D. Naik, A. Rotaru, Y. Garcia, Eur. J. Inorg. Chem. (2011) 3193;
(c) T. Buchen, P. Gütlich, K.H. Sugiyarto, H.A. Goodwin, Chem. Eur. J. 2 (1996) 1134;
(d) K.H. Sugiyarto, M.L. Scudder, D.C. Craig, H.A. Goodwin, Aust. J. Chem. 53 (2000) 755;
(e) Y. Sunatsuki, Y. Ikuta, N. Matsumoto, H. Ohta, M. Kojima, S. Iijima, S. Hayami, Y. Maeda, S. Kaizaki, F. Dahan, J.P. Tuchagues, Angew. Chem., Int. Ed. 42 (2003) 1614;
(f) T. Fujinami, K. Nishi, N. Matsumoto, S. Iijima, M.A. Halcrow, Y. Sunatsuki, M. Kojima, Dalton Trans. 40 (2011) 12301;
(g) K. Nishi, N. Matsumoto, S. Iijima, M.A. Halcrow, Y. Sunatsuki, M. Kojima, Inorg. Chem. 50 (2011) 11303;
(h) D. Furushou, T. Hashibe, T. Fujinami, K. Nishi, H. Hagiwara, N. Matsumoto, Y. Sunatsuki, M. Kojima, S. Iijima, Polyhedron 44 (2012) 194.